Time- and spectrally-resolved four-wave mixing in single CdTe/ZnTe quantum dots

B. Patton and W. Langbein
Department of Physics and Astronomy, Cardiff University, Cardiff CF24 3YB, United Kingdom

U. Woggon
Fachbereich Physik, Universität Dortmund, Otto-Hahn-Strasse 4, 44227 Dortmund, Germany

L. Maingault and H. Mariette
CEA-CNRS research group "Nanophysique et Semiconducteurs" Laboratoire de Spectrometrie Physique, Universite J. Fourier, CEA/DRFMC/SP2M, 17 avenue des Martyrs, 38054 Grenoble, France

(Received 8 February 2006; published 30 June 2006)

We present transient four-wave mixing experiments on individual excitonic transitions in self-assembled CdTe/ZnTe quantum dots. Using a two-dimensional femtosecond spectroscopy and heterodyne detection of the nonlinear signal we study the dephasing and mutual coherent coupling of single quantum dot states. For the homogeneous linewidth of the zero-phonon line (ZPL) values of 0.06–0.1 meV (T_2=13–20 ps) are measured, and a ZPL weight in the total line shape of Z=0.9 at T=7 K is estimated. We observe two linearly polarized fine-structure split exciton transitions with transition dipole moment ratios of 1.0–1.1 deduced from the four-wave mixing (FWM) amplitude, and splitting energies of 0.2–0.35 meV deduced from the FWM spectral response or quantum beat period. Coherent coupling between excitonic states is identified by off-diagonal signals in the two-dimensional spectrally-resolved FWM. The presence of an inhomogeneous broadening caused by spectral diffusion in the time ensemble is evidenced by the formation of a photon echo in the time-resolved FWM from a single transition.

DOI: 10.1103/PhysRevB.73.235354 PACS number(s): 71.35.−y, 78.55.Et, 78.67.Hc

I. INTRODUCTION

Self-assembled quantum dots (QDs) are attractive nanostructures both for fundamental research and device applications. Their discrete energy level structure has made them candidates for use in quantum devices, such as sources of nonclassical light or solid-state quantum logic gates. The development of such QD-based devices has emphasized the need to understand decoherence and radiative lifetimes, fine-structure splitting, mechanisms of coherent coupling, and interaction with the phonon bath. Nonlinear spectroscopy on a single-dot level is a prerequisite for detection, coherent control, and read out of individual quantum states and very sensitive detection techniques need to be developed that allow for the resolution and addressing of single quantum states in both amplitude and phase.[1,2] Most of the reports concerning self-assembled quantum dots deal with III-V materials such as InAs/GaAs for which the existence of quantum islands grown in a Stranski-Krastanov growth mode is well established. Self-assembled quantum dots epitaxially grown in II-VI materials are less explored. With emission energies in the visible range of the spectum, II-VI quantum dots are of great interest as the active medium in optoelectronic devices working in this energy range. As such, understanding the optical properties of excitons trapped by such dots is a necessary prerequisite to further development of technologies based upon these structures. Furthermore, the confinement of excitons in II-VI systems is generally stronger than III-V systems, leading to larger exciton and biexciton binding energies. Thus, concepts of quantum-information processing devices which use exciton-biexciton cascades may work at higher temperatures in II-VI materials. Some results on zero-dimensional structures formed in CdSe/ZnSe structures have been published[3–7] including a coherence study of single self-assembled CdSe QDs.[8]

The formation of Cd-rich dotlike islands in CdTe/ZnTe nanostructures was shown recently by both atomic force microscopy and high resolution transmission electron microscopy,[9] and exciton excited states and fine structure are studied in micro-photoluminescence (μ-PL), PL-excitation spectroscopy, and magneto-optical studies.[9–11] In this work we present transient four-wave mixing (FWM) experiments on individual excitonic transitions in single self-assembled CdTe/ZnTe quantum dots using heterodyne spectral interferometry[1,12] (HSI). We measure the dephasing time and analyze the homogeneous and inhomogeneous broadening of the individual excitonic transitions. Coherent coupling between excitonic states is identified by exploiting the two-dimensional spectrally resolved FWM possible with HSI. The paper is organized as follows: After a short description of sample properties and the experimental setup, we discuss similarities and differences of single dot signals obtained in linear spectroscopy (μ-PL) with those measured by nonlinear spectroscopy (transient FWM). Exploiting polarization-selection rules in FWM we resolve the two linearly-polarized transitions of fine-structure split exciton states and deduce transition dipole moment ratios μ_x/μ_y and exchange splitting energies in Sec. III A. In Sec. III B we discuss the contribution from an acoustic phonon background to the FWM line shape. Then, in Sec. III C we identify the presence of inhomogeneous broadening for individual transitions by the formation of a photon echo in time-resolved FWM, created by the time ensemble over spectral diffusion. Finally, we analyze off-diagonal signatures in the two-dimensional spectrally-resolved FWM signal in Sec. III D and assign them to

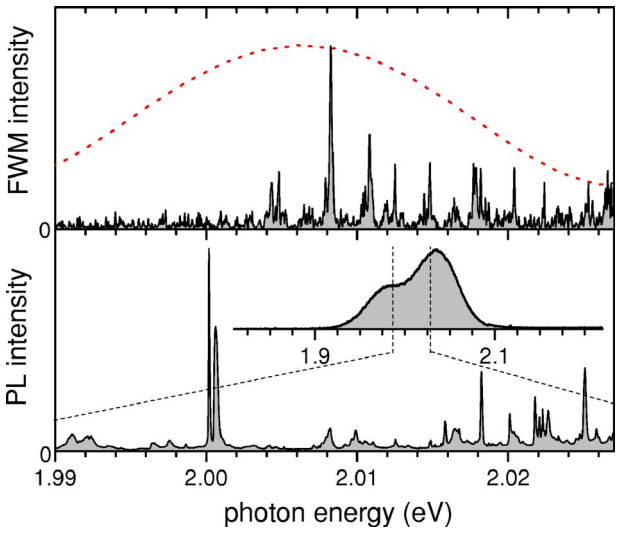

FIG. 1. (Color online) Top: FWM spectrum (solid line) of a $(0.4\ \mu m)^2$ sample region for a delay time $\tau=3$ ps and spectrum of the excitation pulses (dotted line). Bottom: μ-PL from the same sample region. Inset: PL from a larger $(100\ \mu m)^2$ region of the sample.

coherent coupling between intradot exciton or biexciton states.

II. SAMPLES AND EXPERIMENTAL DETAILS

The investigated sample contains self-assembled epitaxial CdTe/ZnTe quantum dots (QDs). Details on the growth and characterization of such structures can be found in Ref. 9. The sample was grown by molecular beam epitaxy on an undoped [001] ZnTe substrate. A ZnTe buffer layer of 500 nm thickness was grown first to spatially separate the QDs from the effects of an eventual contamination of the substrate surface layer. Then, 6 monolayers (ML) of CdTe were grown by atomic layer epitaxy. The morphology transition for the QD formation was induced by a surface energy change affected by deposition of an amorphous Te layer to saturate the surface in the group VI element.[13] After desorbing this amorphous Te layer, the QDs were capped by a 100 nm thick layer of ZnTe. Both surfaces were antireflex coated by a $\lambda/4$ layer (90 nm) of MgO, reducing the reflection around the resonant wavelength of 610 nm below 1%. The sample was mounted in a helium bath cryostat and cooled to a temperature of 7 K. Ensemble photoluminescence spectra of the sample at low excitation intensity shows a QD emission at an energy of 2.02 eV which corresponds to an emission wavelength in the red-spectral range around 610 nm (see inset of Fig. 1). Two peaks are apparent within this ensemble spectrum with a splitting of about 50 meV which are attributed to the presence of a bimodal distribution of dots. The quantum dot density in the investigated sample is several $10^{10}/cm^2$, so that within the spatial resolution of 0.4 μm typically some 10–100 QDs are probed. Due to the large inhomogeneous broadening of about 100 meV, the emission energies of the individual QDs are in general spectrally separated. Photoluminescence (PL) and four-wave mixing (FWM) of individual quantum dots was measured with high spatial resolution of about 0.4 μm given by the diffraction limit of the objective with 0.85 numerical aperture (NA) used to focus the excitation and to collect the signal. The photoluminescence was excited by a continous wave GaN-diode laser (Coherent Radius), emitting at 405 nm.

The FWM experiments were performed using HSI as reported in Refs. 1 and 12. Briefly, we use pulses of 100 fs duration with a repetition rate of 76 MHz from the extracavity frequency doubled signal of an optical parametric oscillator (NT&C 1200X) pumped by a Ti:sapphire oscillator (Coherent Mira). Two pulse trains 1,2 are created by a beam splitter, frequency shifted with acousto-optical modulators (AOMs) and recombined into the same spatial mode, with a relative delay time τ, positive for pulse 1 leading. The pulses are focused onto the sample using a microscope objective mounted in a helium bath cryostat. The FWM signal is collected by the same objective, and directed into a mixing AOM together with a reference beam, in such a way that the diffracted beam of the signal overlaps with the reference beam and vice versa. The mixed beams are spectrally resolved and detected by a liquid nitrogen cooled silicon charge-coupled device (CCD), measuring their spectrally and time-resolved intensities. In this way, the interference frequency of signal and reference fields in the beams is shifted by the mixing AOM drive frequency. We detect the intensities temporally integrated over the 0.1–1 s exposure time of the CCD so that only interference terms around zero frequency are detected. From the measured interference we deduce the signal field in amplitude and phase by spectral interferometry.

When presenting frequency units in the paper we convert them to energy units by multiplying by $\hbar$.

III. RESULTS AND DISCUSSION

Before examining the four-wave mixing response in detail we start with an initial sample characterization and compare the FWM signal to μ-PL experiments on the same sample area. Figure 1 shows the confocally excited/detected PL spectrum of a $(0.4\ \mu m)^2$ area of the CdTe/ZnTe quantum dot sample together with the spectrally resolved FWM intensity obtained from the same sample area. As discussed above, the ensemble PL shows two peaks. When performing FWM experiments we excited in the low energy region of the upper peak as no FWM signal was observed from the lower peak, indicating that the related transitions have a lower transition dipole moment. It is interesting to note that previous studies in CdSe quantum dots[14] showed a strong decrease in the strength of the FWM signal from ensembles with decreasing photon energy. This was so pronounced that the peak of the ensemble PL was the effective lower limit for observing FWM. We see a decrease in the number of states visible in the FWM at the lower energy tail of the ensemble, however we do still see signal. Reference 6 looked at the distribution of luminescence lifetime versus position within the ensemble for CdSe quantum dots and found an increase in lifetime with decreasing emission energy. This was attrib-

uted to a decrease in the coherence volume of the exciton with increasing confinement, resulting in a decreasing radiative lifetime. Thus, it may be possible that there are states with longer coherence times than the ones presented here, which due to the weak transition dipole moment generate FWM signal too weak to be detected with the present setup. A typical PL spectrum of a resolution limited region on the sample is given in the lower part of Fig. 1 for an excitation power of 200 nW. A set of individual emission lines in the PL is observed and attributed to excitonic transitions within individual quantum dots. We note that a possible reason for the different linewidths and shapes can be unintended charging of the QDs, that results in broader emission lines in multiply charged QDs due to final state damping.[15,16]

The same spatial region was investigated with the FWM experiment. The resulting FWM spectral intensity at delay time $\tau=3$ ps is given in the upper part of Fig. 1 along with the spectrum of the excitation pulses. The FWM consists of multiple peaks of some 100 μeV width. While the observed FWM peaks are also present in the PL spectra, their strength does not seem correlated. A similar effect has been observed for localized excitons in GaAs quantum wells.[1] This finding can be related to two origins. First, the spatial resolution of the FWM and the PL data are different. In the FWM, the nonlinearity increases the spatial resolution below the diffraction limit to $0.36\lambda/\mathrm{NA} \approx 260$ nm. In the PL the diffusion of the excited carriers prior to recombination increases the excitation area well above the diffraction limit, so that the PL spatial resolution is determined by the detection resolution of $0.61\lambda/\mathrm{NA}$. The observed area in PL is thus about 3 times larger than in FWM, explaining the occurrence of additional peaks in the PL data. Second, the PL intensity is proportional to the trapping probability of the carriers from the ZnTe barrier into the QDs, while the FWM intensity is proportional to the eight power of the optical transition dipole moment μ of the QD resonance. This explains the missing correlation in the peak intensities of PL and FWM data.

A. Polarization dependence of FWM

Previous studies[9,18] of CdTe dots have shown that individual transitions are often split into orthogonally polarized doublets. As with CdSe QDs[7,19] and InGaAs QDs,[20–23] CdTe dots show an alignment of the linear polarization orientations along the [110] and $[1\bar{1}0]$ crystal directions.[11,24] These are the anisotropy axes of the surface diffusion during growth as well as the (in plane) anisotropy axes of the T_d crystal symmetry leading to piezoelectric fields.[17]

While the exchange splitting *energies* can be inferred directly from the peak positions in emission for the two linearly polarized exciton transitions, the *transition dipole moments* can not be determined from a photoluminescence spectrum only. A FWM experiment instead is sensitive to the transition dipole moments, and allows us to measure the optical transition dipole matrix elements μ_x and μ_y of the two states of the exciton doublet,[25] where x,y label[17] the two orthogonal directions [110] and $[1\bar{1}0]$. We therefore exploit polarization selection rules in single-dot FWM experiments to determine exchange splitting energies and ratios μ_x/μ_y for the single exciton fine structure in CdTe/ZnTe QDs.

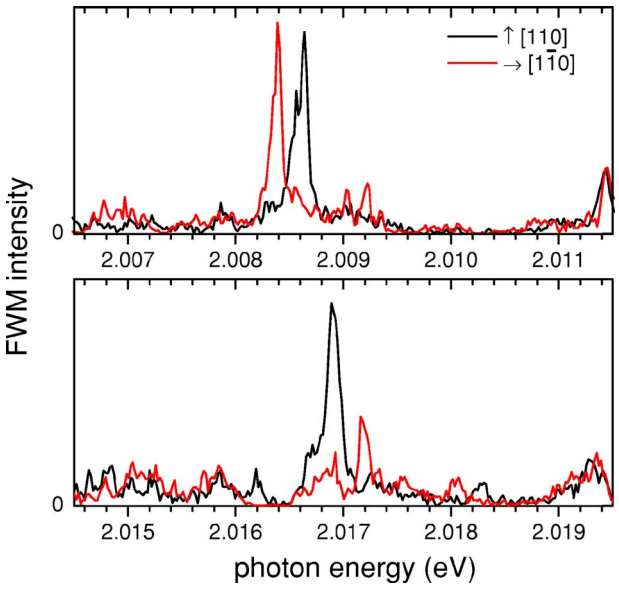

FIG. 2. (Color online) FWM spectra for a delay time $\tau=2$ ps for two orthogonal linear excitation polarizations along the [110] (black) and $[1\bar{1}0]$ [red (gray)] crystal direction (Ref. 17). The upper and lower graph are taken on different sample positions, each featuring an individual resonance.

In order to control the excitation and detection polarization, we inserted a $\lambda/2$ wave plate in front of the microscope objective (see setup in Refs. 1 and 12). By rotating the wave plate, the direction of the linear excitation polarization on the sample is rotated by twice the angle. The detection polarization is rotated in the same way since the detected FWM signal travels back through the wave plate. Figure 2 shows the measured FWM spectra for wave plate rotations of 0 and 45° relative to the incoming linearly polarized excitation for two different quantum dots. The QD in the upper panel shows two equally strong signals for the two polarizations, split by 0.22 ± 0.02 meV. This splitting is within the range observed in previous PL studies on such QDs.[9] The QD in the lower panel shows a similar splitting of 0.3 ± 0.02 meV, but furthermore a significant difference in the FWM signal strength. This we interpret as a difference in the transition dipoles $\mu_{x,y}$ of the two transitions. Since the FWM intensity is proportional to μ^8, we can estimate for this lower dot $\mu_x/\mu_y=1.11\pm0.02$. A similar observation of anisotropy of the transition dipoles of excitonic transitions has been made on InGaAs quantum dots.[25,26] The difference in oscillator strength is, as the fine-structure splitting itself, related to the in-plane asymmetry of the QD confinement potential, mixing electronic states of p symmetry into the s-like exciton ground state, and mixing light-hole components into the lowest confined hole state that has, in absence of asymmetry, pure heavy-hole character.[22,23] The direct access to the optical transition dipole matrix element in single-dot FWM should enable a better comparison of the fine-structure splitting with theoretical predictions for different microscopic origins in the future.

B. Acoustic-phonon assisted transitions in the FWM of single exciton states

Excitons that are localized to a small volume of less than about $(10\ \mathrm{nm})^3$ tend to show a significant strength of acoustic phonon-assisted transitions in their absorption and emission line shapes,[27–30] which can be theoretically described[31,32] within the independent boson model. The consequence of these phonon-assisted transitions in four-wave mixing experiments on ensembles of InGaAs QDs[33–35] is an initial fast decay on the picosecond time scale, followed by a slow decay of the zero-phonon line (ZPL) on the nanosecond time scale. In the spectral domain this corresponds to a non-Lorentzian line shape with a sharp (μeV) ZPL superimposed on a broad (meV) acoustic phonon background. With increasing temperatures, the relative contribution of the acoustic phonon background increases, and its asymmetry diminishes. While such line shapes have been observed in the PL of single QDs,[27–29,36] FWM experiments were limited to ensemble studies. Here, we attempt to study the FWM spectral line shape of a single QD, which was theoretically discussed in Ref. 37. It is expected that the weight of the phonon-assisted transitions in the FWM line shape is similar to the one in the linear response observable in absorption, both line shapes are actually equal for $\tau=0$. The FWM spectrum, however, develops from an asymmetric shape at $\tau=0$ (pronounced at low temperatures) to a symmetric one for larger delays (see Fig. 3 in Ref. 37).

To investigate this behavior experimentally, we measured the FWM response of a single exciton transition as a function of delay τ. The resulting spectrally resolved FWM intensity is given in the top of Fig. 5. It consists of a dominating resonance at 2.0085 eV, and some additional weaker ones at other energies. The difficulty of measuring the acoustic-phonon band is evident: Due to its large linewidth compared to the zero-phonon line, its spectral intensity is expected to be about 2–3 orders of magnitude weaker than the ZPL. It is therefore a challenge to detect the acoustic phonon band within the dynamic range of single QD FWM experiments. In the measurement, a spectrally broad response for small delay times $0 \leqslant \tau \leqslant 3$ ps is visible, which could be due to the phonon bands of all participating transitions (see Fig. 3 top). The delay-dependent FWM intensity, averaged over 0.4 meV (open squares) or 4 meV (solid triangles) around the ZPL peak, is given in the inset of Fig. 3. The narrow averaging, which essentially represents the ZPL intensity, shows an approximately exponential decay. For a homogeneously broadened resonance, this decay is interpreted as $\propto \exp(-2\tau/T_2)$ with a dephasing time $T_2 = 13 \pm 3$ ps. This agrees with the results obtained through FWM upon ensembles of CdTe QDs described in Ref. 38. The resulting homogeneous linewidth of $2/T_2 = 0.1$ meV is equal to the measured FWM linewidth, confirming the assumption of dominant homogeneous broadening. This dephasing time is significantly shorter than the typical PL emission lifetime after nonresonant excitation of 100–200 ps,[9,39] indicating that the dephasing time might not be radiatively limited, as opposed to the dephasing in InGaAs QDs.[25] However, the radiative lifetime in the investigated CdTe QDs is not well known, and it can in principle take values between the radiative lifetime of excitons in ideal CdTe quantum wells of about 1 ps and the strong confinement limit in the nanosecond range, depending on the size of the localized exciton wavefunction. In CdSe QDs, a related strong dependence of the radiative lifetime on the confinement energy was found.[6] Additionally, we need to consider that the FWM signal intensity scales with the fourth power of the radiative decay rate, so that we will preferentially select states with short radiative lifetimes in our experiment. For comparison, excitons in GaAs quantum wells have radiative lifetimes of 10–30 ps and excitons localized in interface fluctuations[1] show dephasing times of 20–50 ps, close to the quantum well value, indicating a weak confinement.

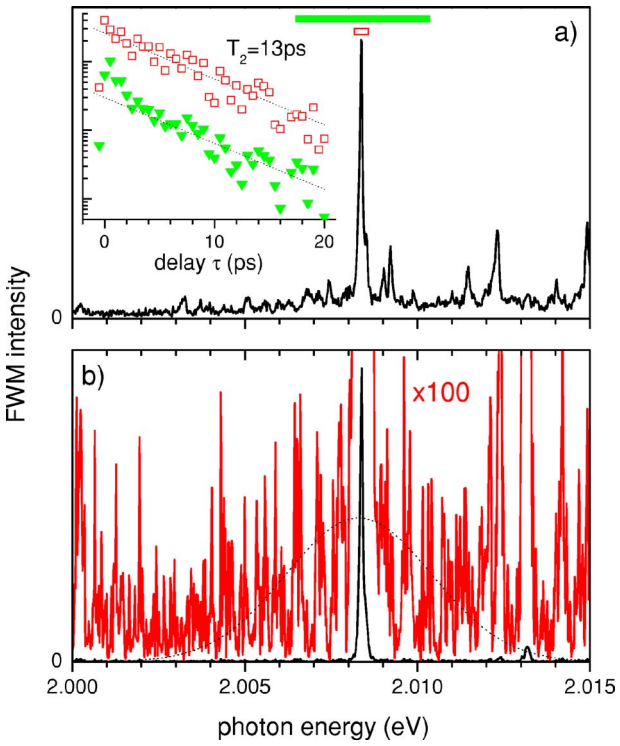

FIG. 3. (Color online) Top: FWM intensity averaged over $\tau = 0-3$ ps. Inset: FWM intensity averaged over 0.4 meV (open squares) and 4 meV (filled triangles) around the resonance as function of delay τ. The green (solid) and red (hollow) bars on top indicate the averaging ranges. Bottom: Intensity of the FWM field averaged over $\tau = 3-20$ ps. Red (gray) line: magnified by a factor of 100. Dotted line: estimated shape of the acoustic phonon band.

The dynamics for wide averaging instead shows in addition to the exponential decay an initial fast decay as expected for the phonon-assisted processes. The theory, however, does not predict such a difference in the delay dynamics of the ZPL and the phonon band. We therefore presume that most of the fast decaying FWM intensity is not related to the phonon band of the dominating transition. Its origin could be the phonon bands of the other transitions overlapping spectrally, or resonances with fast dephasing unrelated to the phonon band. The observation of the phonon-related fast initial decay, which was clearly resolved in measurements of ensembles of InGaAs QDs,[35] is hampered here by the noise in the FWM intensity. The expected decay within the first picoseconds is by a factor of Z^3, where Z is the ZPL fraction of

the transition in linear response.[34,35] From the intensity noise of the measured delay-time dynamics, we can estimate a lower bound of 0.85 for Z (at a lattice temperature of 7 K).

For longer delay times, the phonon-assisted line shape is expected to be constant,[37] since the FWM is created only by the remaining ZPL polarization created by pulse 1. We can therefore increase the dynamic range of the measurement by summing the measured FWM field for different delay times, prior to which the FWM field phase has been normalized to the phase at the ZPL. This procedure is equal to taking the later discussed two-dimensional FWM intensity $I(\omega,\omega_1)$ at ω_1 equal to the ZPL resonance. The result is given in Fig. 3 (bottom). The additional peak at 2.013 eV is due to a coherently coupled transition, as discussed later. When magnifying the background by a factor of 100, a broad signal around the ZPL emerges. While the data does not allow the extraction of a line shape of the broad band, which is expected to be similar to the dotted line, the intensity of the background spectrally integrated in a range of 5 meV around the ZPL allows us to estimate the ZPL weight in the total line shape to be $Z \approx 0.9$, which is similar to the results of PL experiments on similar QDs.[29,40] It is also consistent with the lower limit of 0.85 estimated from the delay-time dependence of the ZPL FWM intensity, as discussed above. It might be expected that the exciton states best observable in FWM are the ones with the weakest phonon band, since a strong FWM implies a large transition dipole moment, which in turn implies a large coherence volume and thus a large wave function size.

C. Homogenous and inhomogenous broadening of single exciton states

Probing an ensemble of resonance energies in FWM leads to the formation of a photon echo due to the phase conjugation of the first-order polarization created by pulse 1 in the FWM field. This is a well known feature and has been observed first in spin echoes,[41] and later also in the optical frequency range.[42] Since in the photon echo all resonances emit the FWM polarization in phase, the delay-time dependence of the photon echo intensity gives a direct measure of the homogeneous broadening of the resonances even in presence of a much broader distribution of resonance energies. This was widely used to measure dephasing times in inhomogeneously broadened exciton ensembles, see, e.g., Ref. 43. In more recent experiments the inhomogeneous broadening was resolved by measuring small ensembles using high spatial resolution. In such experiments, the measurement time has to be much longer than the dephasing time in order to collect a sufficient number of photons. During this time, fluctuations of the environment can lead to slow spectral diffusion of the frequency of the investigated transitions (e.g., by the Stark effect), resulting in an inhomogeneous broadening in the measurement due to the time ensemble.[44] As a result, the typical linewidth of individual semiconductor quantum dots at low temperatures measured in single-dot photoluminescence are 100–1000 μeV,[9,19,45–48] much larger than the homogeneous linewidth as determined in large ensemble photon echo experiments.[33,49] In a recent work[1] we have shown how the photon echo forms in small ensembles. Here we want to concentrate on the inhomogeneous broadening of a single exciton transition due to the time ensemble of spectral wandering.

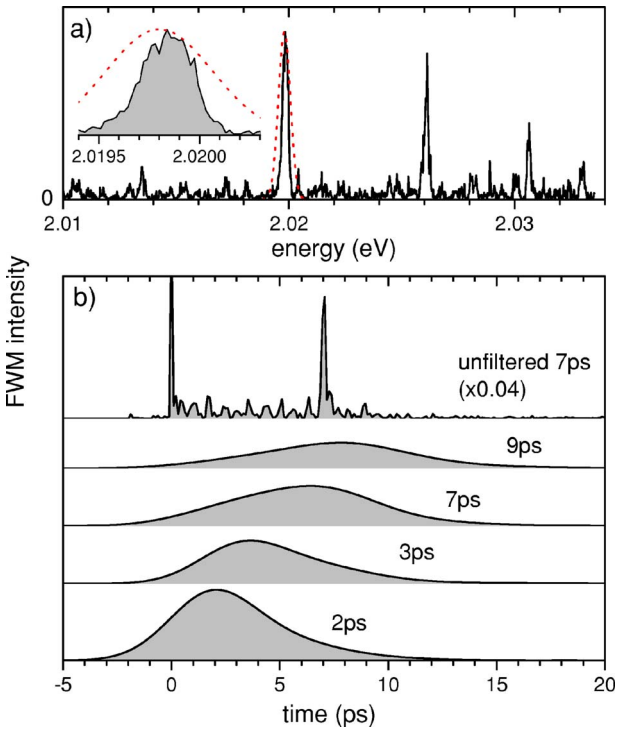

FIG. 4. (Color online) Photon echo formation from a single exciton transition. (a) Spectrally resolved FWM intensity from multiple states at $\tau=7$ ps. The inset shows the broadening of a single transition. The dotted line shows the filter functions used to isolated the single transition. (b) Time-dependent FWM for this single transition at various delays τ. Also shown for comparison is the unfiltered FWM at $\tau=7$ ps.

The spectral FWM intensity from a sample region with exciton states of significant linewidth (and hence ones expected to show effects from spectral wandering) is given in Fig. 4(a). The inset magnifies a line-shape of about 0.35 meV full width at half maximum (FWHM), which is much larger than the width of 0.1 meV for the homogeneously broadened transition discussed is the previous section. The time-dependent FWM [uppermost line in Fig. 4(b)] shows the expected echo at the delay time, $\tau=7$ ps created by the probed ensemble of a few transitions. The signal at $t=0$ is attributed to an artifact of the probe pulse. To investigate the time evolution of the FWM from a single transition, we spectrally filter the FWM around the transition [see Fig. 4(a)] with a Gaussian of 0.62 meV FWHM. The resulting time evolution of the FWM intensity is given in Fig. 4(b) for various delay times. A shift of the FWM with increasing delay time is observed. The transition thus does show a photon echo as opposed to a free polarization decay, indicating that it is dominantly inhomogeneously broadened. The origin of this broadening is most likely the quantum confined Stark effect of fluctuating local electric fields. The homogeneous broadening of the transition is consequently estimated from the decay of the photon echo intensity with delay time

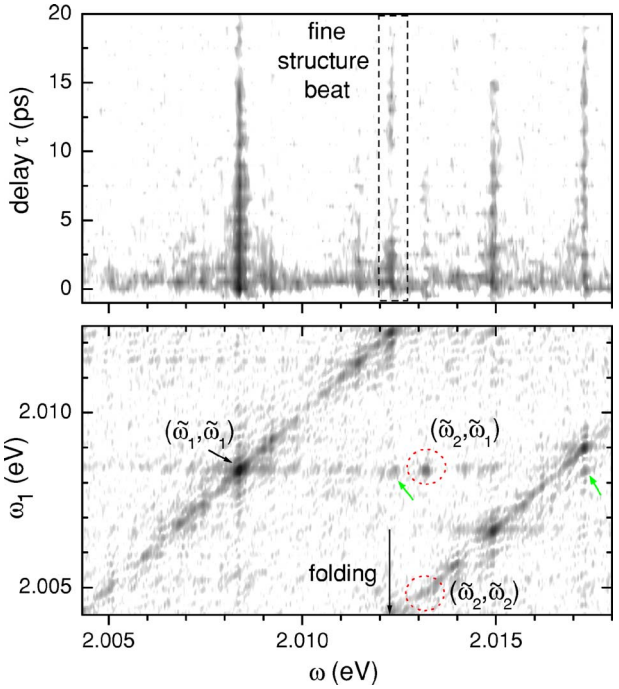

FIG. 5. (Color online) Top: spectrally resolved FWM intensity $I(\omega,\tau)$ versus delay time τ. Logarithmic gray scale over 2 orders of magnitude. The fine-structure beat shown in Fig. 6 is indicated. Bottom: Two-dimensional spectrally resolved FWM intensity $I(\omega,\omega_1)$. Logarithmic gray scale over 3 orders of magnitude.

$\propto \exp(-4\tau/T_2)$, resulting in $T_2=20\pm5$ ps or a FWHM of $2/T_2=66$ μeV.

D. Coherent coupling between dot states

The FWM as function of delay τ can reveal coherent coupling between excitonic states, which is normally observed as beating of the intensity versus delay time. The phase information which is recovered with the HSI technique allows the Fourier transformation of the FWM field along the delay, thereby creating a two-dimensional spectrally resolved FWM intensity $I(\omega,\omega_1)$ that is particularly useful to analyze coherent coupling between states.[50,51] Transforming the delay time τ into the first-order frequency ω_1 allows us to detect very weak oscillatory components without the background of the uncoupled response. The upper part of Fig. 5 shows a measured spectrally resolved FWM intensity $I(\omega,\tau)$ versus delay on the sample area used also for Fig. 3. In order to perform the transform from τ to ω_1, we have to know the relative phases of the FWM fields measured for different delay times. We determine the relative phases here by choosing a strong FWM resonance at $\omega=\tilde{\omega}_1$. Assuming the absence of significant coherent coupling in this transition, the phase evolution of the resonant FWM is given by $\exp(-i\tilde{\omega}_1\tau)$, to which we adjust the measured phase evolution. The resulting transformed $I(\omega,\omega_1)$ is given in the lower part of Fig. 5 on a logarithmic gray scale over three orders of magnitude. The dynamic range has improved since the signal is concentrated into peaks in both dimensions, which indicate the frequencies of the participating transitions. As the data is taken for delays on a equidistant grid of step size Δ_τ, the discrete Fourier transform creates a ω_1 frequency span of $\Delta=2\pi/\Delta_\tau$, into which all components are shifted modulo Δ. The used step size of $\Delta_\tau=0.5$ ps results in a frequency range of $\Delta=8.3$ meV. The measured $I(\omega,\omega_1)$ is dominated by the signal on the diagonal $\omega=\omega_1$. The frequency jump of ω_1 by Δ in the data is visible at $\omega=2.0125$ eV, indicated by the arrow "folding." For a more detailed discussion see Ref. 12.

In a multilevel system with transition frequencies $\tilde{\omega}_k$ and dipole moments μ_k, the third-order polarization for positive delay times neglecting damping can be written as

$$P^{(3)}(t>0,\tau>0)\propto\sum_{k\in X}\mu_k e^{-i\tilde{\omega}_k\tau}\left(\sum_l \mu_l A_{kl} e^{i\tilde{\omega}_l t}\right), \quad (1)$$

where A_{kl} describes the polarization transfer between the transitions k and l via the second excitation field. X denotes the excitonic transitions, i.e., from the crystal ground state to a single electron-hole pair. Fourier transforming $t\rightarrow\omega$ and $\tau\rightarrow\omega_1$ gives

$$P^{(3)}(\omega,\omega_1)\propto\sum_{k\in X}\mu_k\delta(\omega_1+\tilde{\omega}_k)\left(\sum_l \mu_l A_{kl}\delta(\omega-\tilde{\omega}_l)\right). \quad (2)$$

For uncoupled two-level systems $A_{kl}=\delta_{kl}\mu_k\mu_l$ holds, so that only peaks along $\omega_1=\omega$ are present. Coupled transitions $k\neq l$ instead create off-diagonal peaks at $(\omega,\omega_1)=(\tilde{\omega}_l,\tilde{\omega}_k)$. The actual spectral width of the peaks in the experiment is determined by the respective dephasing of the involved transitions. Apart from the peaks on the diagonal indicating uncoupled transitions, a nondiagonal peak in $I(\omega,\omega_1)$ at $(\tilde{\omega}_2,\tilde{\omega}_1)=(2.0132,2.0083)$ eV is observed, indicated by a circle. The transition $\tilde{\omega}_2$ is not pronounced on the diagonal position $(\tilde{\omega}_2,\tilde{\omega}_2)$. We propose two possible explanations for the occurrence of signal at $(\tilde{\omega}_2,\tilde{\omega}_1)=(2.0132,2.0083)$ eV: (i) $\tilde{\omega}_2$ could be an exciton-biexciton transition, which does not appear on the diagonal. The energy splitting between $\tilde{\omega}_1$ and $\tilde{\omega}_2$ of -5 meV would be the related negative biexciton binding energy, inconsistent with the positive biexciton binding energies observed in all previous studies on similar CdTe QDs.[10,38,40] These studies found a biexciton binding energy of 13 meV which was observed in ensemble FWM experiments as a beat with a 320 ps period. Such an exciton-biexciton transition could be seen in our experiment refolded back into the repeat period of ω_1. We have not observed any such peaks of significant strength (also at the expected ω positions 13 meV below $\tilde{\omega}_{1,3}$, outside of the range displayed in Fig. 5). (ii) $\tilde{\omega}_2$ could be a transition to an excited state in the same QD as $\tilde{\omega}_1$ with a weak μ_2. In this case, the transition should be present on the diagonal, but might be within the noise since the FWM intensity scales as $\mu_k^4\mu_l^4$. The FWM intensity at $(\tilde{\omega}_2,\tilde{\omega}_1)$ is 16 times weaker than at $(\tilde{\omega}_1,\tilde{\omega}_1)$, so that we can estimate $\mu_2/\mu_1\approx2$, leading to a diagonal signal at $(\tilde{\omega}_2,\tilde{\omega}_2)$ that is 250 times weaker than at $(\tilde{\omega}_1,\tilde{\omega}_1)$. This is actually close to the noise level of the measurement, and we cannot conclusively decide between the two cases for now. We observe other weak nondiagonal components in $I(\omega,\omega_1)$ coupling the major diagonal resonances, indicated by the green arrows in Fig. 5. These can be attributed to a weak dipole-dipole coupling between the resonances. From the

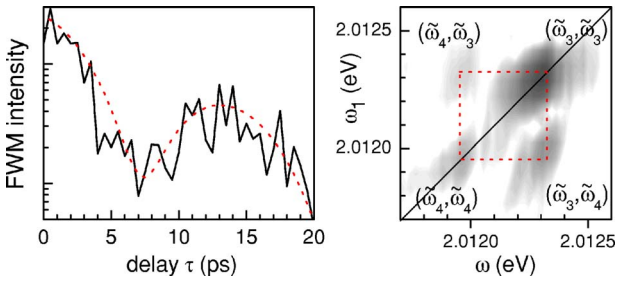

FIG. 6. (Color online) Left: Delay time cut along $\omega = 2.0123$ eV showing beating with a period of 14 ps (solid line). Dashed line shows a fit using Eq. (3). Right: Two-dimensional spectrally resolved FWM intensity $I(\omega, \omega_1)$ about the relevant spectral region. Logarithmic gray scale over 2 orders of magnitude.

nondiagonal intensities, we can estimate the interaction strength to about 1–10 % of the linewidth, i.e. 1–10 μeV. These values are in the range theoretically expected both for radiative coupling via the transition dipole[52] and for coupling via the static dipole moment of the excitons.[53] A three-beam FWM experiment to measure the density lifetime of the coupling could distinguish between the effects: For radiative coupling the related density is in the exciton that emits the FWM polarization, while for static coupling the density is in the coupled exciton. Comparing the nondiagonal lifetime with the two diagonal lifetimes identifies the exciton that carries the coupling-related density.

One beat structure with a long period is already visible in the delay resolved FWM $I(\omega, \tau)$ at $\omega = \tilde{\omega}_3 = 2.0123$ eV. The measured $I(\tau, \tilde{\omega}_3)$ is given on the left graph of Fig. 6, along with the fit function

$$I(\tau) = Ae^{-2\pi/T_2}\left[1 + B\cos\left(\frac{2\pi\tau}{t_{\text{osc}}}\right)\right], \tag{3}$$

where $t_{\text{osc}} = 14.5$ ps is the period of oscillation of the coupled system, and $T_2 = 16$ ps. The oscillation contrast $B = 0.8$ is not unity, indicating different transition dipole moments of the two transitions. From the period we estimate a related splitting of $h/t_{\text{osc}} = 0.29$ meV. Figure 6 (right) shows a view of the corresponding region in $I(\omega, \omega_1)$. Here the related resonances can be observed, revealing the second resonance energy $\tilde{\omega}_4 = 2.011\,95$ eV with a splitting of 0.35 meV to $\tilde{\omega}_3$. The presence of the two off-diagonal peaks at $(\tilde{\omega}_4, \tilde{\omega}_3)$ and $(\tilde{\omega}_3, \tilde{\omega}_4)$ showing the coupling of the states are also observed. Considering the size of the splitting, we attribute $\tilde{\omega}_3, \tilde{\omega}_4$ to a pair of fine-structure split exciton transitions. We can estimate $\mu_4/\mu_3 \approx 0.6$ for the linear polarization used in the experiment from the FWM intensities. The fact that all four components of the coupled system are so clearly visible highlights the effectiveness of the Fourier transform technique in maximizing the dynamic range of the data.

IV. CONCLUSIONS

We have shown that with the sensitivity of HSI it is possible to perform four-wave mixing experiments on single self-organized CdTe quantum dots. The recovered signal is sufficient to allow investigation of such dot parameters as anisotropy, excitonic coupling to acoustic phonons, and coherent coupling between different intradot states. We also showed that the time ensemble used by the measurement technique allows the observation of a photon echo from individual excitonic states.

ACKNOWLEDGMENTS

This work was funded by the German Science Foundation (DFG) within the Grant WO477/14 and by the UK Engineering and Physical Sciences Research Council within the Grant EP/D025303/1.

[1] W. Langbein and B. Patton, Phys. Rev. Lett. **95**, 017403 (2005).
[2] B. Patton, U. Woggon, and W. Langbein, Phys. Rev. Lett. **95**, 266401 (2005).
[3] S. H. Xin, P. D. Wang, A. Yin, C. Kim, M. Dobrowolska, J. L. Merz, and J. K. Furdyna, Appl. Phys. Lett. **69**, 3884 (1996).
[4] M. Lowisch, M. Rabe, B. Stegemann, F. Henneberger, M. Grundmann, V. Türck, and D. Bimberg, Phys. Rev. B **54**, R11074 (1996).
[5] K. Leonardi, K. Ohkawa, D. Hommel, H. Selke, F. Gindele, and U. Woggon, Appl. Phys. Lett. **71**, 1510 (1997).
[6] F. Gindele, U. Woggon, W. Langbein, J. M. Hvam, K. Leonardi, D. Hommel, and H. Selke, Phys. Rev. B **60**, 8773 (1999).
[7] V. D. Kulakovskii, G. Bacher, R. Weigand, T. Kümmell, A. Forchel, E. Borovitskaya, K. Leonardi, and D. Hommel, Phys. Rev. Lett. **82**, 1780 (1999).
[8] T. Flissikowski, A. Hundt, M. Lowisch, M. Rabe, and F. Henneberger, Phys. Rev. Lett. **86**, 3172 (2001).
[9] L. Marsal, L. Besombes, F. Tinjod, K. Kheng, A. Wasiela, B. Gilles, J.-L. Rouvière, and H. Mariette, J. Appl. Phys. **91**, 4936 (2002).
[10] L. Besombes, K. Kheng, L. Marsal, and H. Mariette, Europhys. Lett. **65**, 144 (2004).
[11] L. Besombes, K. Kheng, and D. Martrou, Phys. Rev. Lett. **85**, 425 (2000).
[12] W. Langbein and B. Patton, Opt. Lett. **31**, 1151 (2006).
[13] F. Tinjod, B. Gilles, S. Moehl, K. Kheng, and H. Mariette, Appl. Phys. Lett. **82**, 4340 (2003).
[14] H. P. Wagner, H.-P. Tranitz, H. Preis, W. Langbein, K. Leosson, and J. M. Hvam, Phys. Rev. B **60**, 10640 (1999).
[15] I. A. Akimov, A. Hundt, T. Flissikowski, and F. Henneberger, Appl. Phys. Lett. **81**, 4730 (2002).
[16] B. Urbaszek, R. J. Warburton, K. Karrai, B. D. Gerardot, P. M. Petroff, and J. Garcia, Phys. Rev. Lett. **90**, 247403 (2003).
[17] We could only determine the orthogonal directions [110] and $[1\bar{1}0]$ by the orthogonal cleavage facets of the crystal. This leaves an ambiguity in the ordering.
[18] K. P. Hewaparakrama, A. W. S. Mackowski, H. E. Jackson, L. M.

Smith, G. Karczewski, and J. Kossut, Appl. Phys. Lett. **85**, 5463 (2004).
[19] B. Patton, W. Langbein, and U. Woggon, Phys. Rev. B **68**, 125316 (2003).
[20] M. Bayer, G. Ortner, O. Stern, A. Kuther, A. A. Gorbunov, A. Forchel, P. Hawrylak, S. Fafard, K. Hinzer, T. L. Reinecke, S. N. Walck, J. P. Reithmaier, F. Klopf, and F. Schäfer, Phys. Rev. B **65**, 195315 (2002).
[21] W. Langbein, P. Borri, U. Woggon, V. Stavarache, D. Reuter, and A. D. Wieck, Phys. Rev. B **69**, 161301(R) (2004).
[22] R. Seguin, A. Schliwa, S. Rodt, K. Pötschke, U. W. Pohl, and D. Bimberg, Phys. Rev. Lett. **95**, 257402 (2005).
[23] R. J. Young, R. M. Stevenson, A. J. Shields, P. Atkinson, K. Cooper, D. A. Ritchie, K. M. Groom, A. I. Tartakovskii, and M. S. Skolnick, Phys. Rev. B **72**, 113305 (2005).
[24] S. Mackowski, T. A. Nguyen, T. Gurung, K. Hewaparakrama, H. E. Jackson, L. M. Smith, J. Wrobel, K. Fronc, J. Kossut, and G. Karczewski, Phys. Rev. B **70**, 245312 (2004).
[25] W. Langbein, P. Borri, U. Woggon, V. Stavarache, D. Reuter, and A. D. Wieck, Phys. Rev. B **70**, 033301 (2004).
[26] A. Muller, Q. Q. Wang, P. Bianucci, C. K. Shih, and Q. K. Xue, Appl. Phys. Lett. **84**, 981 (2004).
[27] L. Besombes, K. Kheng, L. Marsal, and H. Mariette, Phys. Rev. B **63**, 155307 (2001).
[28] E. Peter, J. Hours, P. Senellart, A. Vasanelli, A. Cavanna, J. Bloch, and J. M. Gérard, Phys. Rev. B **69**, 041307(R) (2004).
[29] S. Moehl, F. Tinjod, K. Kheng, and H. Mariette, Phys. Rev. B **69**, 245318 (2004).
[30] P. Palinginis, H. Wang, S. V. Goupalov, D. S. Citrin, M. Dobrowolska, and J. K. Furdyna, Phys. Rev. B **70**, 073302(R) (2004).
[31] B. Krummheuer, V. M. Axt, and T. Kuhn, Phys. Rev. B **65**, 195313 (2002).
[32] B. Krummheuer, V. M. Axt, T. Kuhn, I. DAmico, and F. Rossi, Phys. Rev. B **71**, 235329 (2005).
[33] P. Borri, W. Langbein, S. Schneider, U. Woggon, R. L. Sellin, D. Ouyang, and D. Bimberg, Phys. Rev. Lett. **87**, 157401 (2001).
[34] A. Vagov, V. M. Axt, T. Kuhn, W. Langbein, P. Borri, and U. Woggon, Phys. Rev. B **70**, 201305(R) (2004).
[35] P. Borri, W. Langbein, U. Woggon, V. Stavarache, D. Reuter, and A. D. Wieck, Phys. Rev. B **71**, 115328 (2005).
[36] I. Favero, G. Cassabois, R. Ferreira, D. Darson, C. Voisin, J. Tignon, C. Delalande, G. Bastard, P. Roussignol, and J. M. Gérard, Phys. Rev. B **68**, 233301(R) (2003).
[37] A. Vagov, V. M. Axt, and T. Kuhn, Phys. Rev. B **67**, 115338 (2003).
[38] Y. Viale, P. Gilliot, O. Crégut, J.-P. Likforman, B. Hönerlage, R. Levy, L. Besombes, L. Marshal, K. Kheng, and H. Mariette, Mater. Sci. Eng., B **101**, 55 (2003).
[39] C. Couteau, S. Moehl, F. Tinjod, J. M. G'erard, K. Kheng, H. Mariette, J. A. Gaj, R. Romestain, and J. P. Poizat, Appl. Phys. Lett. **85**, 6251 (2004).
[40] L. Besombes, K. Kheng, L. Marsal, and H. Mariette, Phys. Rev. B **65**, 121314(R) (2002).
[41] E. L. Hahn, Phys. Rev. **80**, 580 (1950).
[42] N. A. Kurnita, I. D. Abella, and S. R. Hartmann, Phys. Rev. Lett. **13**, 567 (1964).
[43] J. Shah, in *Ultrafast Spectroscopy of Semiconductors and Semiconductor Nanostructures* (Springer, Berlin, 1996), Chap. 2.
[44] S. Mukamel, *Principles of Nonlinear Optical Spectroscopy* (Oxford, New York, 1999).
[45] S. A. Empedocles, D. J. Norris, and M. G. Bawendi, Phys. Rev. Lett. **77**, 3873 (1996).
[46] B. P. Zhang, Y. Q. Li, T. Yasuda, W. X. Wang, Y. Segawa, K. Edamatsu, and T. Itoh, Appl. Phys. Lett. **73**, 1266 (1998).
[47] J. Seufert, R. Weigand, G. Bacher, T. Kummell, and A. Forchel, Appl. Phys. Lett. **76**, 1872 (2000).
[48] V. Türck, S. Rodt, O. Stier, R. Heitz, R. Engelhardt, U. W. Pohl, D. Bimberg, and R. Steingrüber, Phys. Rev. B **61**, 9944 (2000).
[49] R. Kuribayashi, K. Inoue, K. Sakoda, V. A. Tsekhomskii, and A. V. Baranov, Phys. Rev. B **57**, R15084 (1998).
[50] S. Mukamel, Annu. Rev. Phys. Chem. **51**, 691 (2000).
[51] T. Brixner, J. Stenger, H. M. Vaswani, M. Cho, R. E. Blankenship, and G. R. Fleming, Nature (London) **434**, 625 (2005).
[52] G. Parascandolo and V. Savona, Phys. Rev. B **71**, 045335 (2005).
[53] T. Unold, K. Mueller, C. Lienau, T. Elsaesser, and A. D. Wieck, Phys. Rev. Lett. **94**, 137404 (2005).